Journal of Catalysis **204,** 440–449 (2001)
doi:10.1006/jcat.2001.3403, available online at http://www.idealibrary.com on IDEAL®

A Kinetic Study of the Thermal and Photochemical Partial Oxidation of Cyclohexane with Molecular Oxygen in Zeolite Y

R. G. Larsen, A. C. Saladino, T. A. Hunt, J. E. Mann, M. Xu, V. H. Grassian,[1] and S. C. Larsen[1]

Department of Chemistry, University of Iowa, Iowa City, Iowa 52242

Received May 22, 2001; revised August 29, 2001; accepted August 29, 2001

The kinetics of the thermal and photochemical oxidation of cyclohexane in zeolite Y were investigated using *ex situ* GC product analysis and *in situ* FTIR and solid state NMR spectroscopies. The results show that cyclohexyl hydroperoxide, cyclohexanone, and cyclohexanol (and water) are formed during the thermal and photochemical oxidation of cyclohexane in BaY. The overall percent conversion of cyclohexane decreases dramatically at cyclohexane loadings of greater than 3 cyclohexane molecules per supercage. Pronounced deuterium kinetic isotope effects were observed for both the thermal and photochemical cyclohexane oxidation reactions, indicating that a proton transfer step is a rate-limiting step in the reaction mechanism. For the thermal oxidation of cyclohexane in BaY and NaY, activation energies of 62 (±9) and 85 (±3) kJ/mol, respectively, were measured.

INTRODUCTION

The partial oxidation of hydrocarbons is significant to the chemical industry because these oxidation reactions are used to convert petroleum hydrocarbon feedstocks into chemicals important in the polymer and petrochemical industries. Liquid phase air oxidations are generally preferred by the chemical industry because of the mild reaction conditions (1). However, conversions of the oxidation processes are typically very low in order to maintain high selectivity. This is necessary because the desired partial oxidation products can easily be further oxidized under typical reaction conditions. Current liquid phase methods for the autooxidation of cyclohexane using soluble cobalt or manganese catalysts only exhibit acceptable product selectivity (>80%) when cyclohexane conversion is very low (<5%) (2, 3). Although more efficient processes are known, economic and safety considerations strongly favor oxidants, such as air or oxygen for use in large-scale production, and have lead to the large-scale adoption of a cost effective, yet seemingly inefficient production process.

The inefficiency associated with low conversion and the need to separate catalyst from products has motivated the search for solid catalysts that are active for the oxidation of cyclohexane (4–10). Frei and coworkers demonstrated that the oxidation of cyclohexane to cyclohexanone with molecular oxygen occurs with very high selectivity under mild thermal and photochemical conditions in cation-exchanged zeolites, such as NaY (10–12). Figure 1 shows a Y zeolite with one molecule of adsorbed cyclohexane and illustrates the relative sizes of cyclohexane and zeolite Y pores. An additional benefit of this approach is that the oxidation of cyclohexane by molecular oxygen in NaY is desirable from an environmental perspective; the high selectivity minimizes waste, and the process utilizes the clean and inexpensive oxidant, molecular oxygen.

Frei and coworkers proposed a reaction mechanism for the oxidation of cyclohexane in NaY that involved a charge transfer complex, $[(\text{cyclohexane})^+\ O_2^-]$, as follows (10, 12–15):

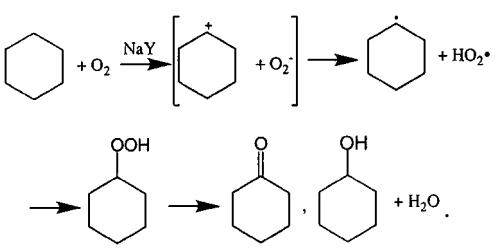

[1]

The hypothesis is that the charge transfer complex is stabilized by the exchangeable cation in the zeolite and that this stabilization allows access to the charge transfer state by visible light irradiation or by thermal activation. In the next step of the reaction, a proton from the cyclohexane cation radical is abstracted by O_2^- to form HO_2 and a cyclohexyl radical. The HO_2 radical attacks the cyclohexyl radical to form cyclohexyl hydroperoxide under both photochemical and thermal conditions. Using Fourier transform infrared (FTIR) spectroscopy, the formation of cyclohexyl hydroperoxide, which reacts thermally to form cyclohexanone and water, was observed (10). Complete selectivity in the photooxidation of cyclohexane to cyclohexanone was reported at conversions as high as 40%, based on *in situ* FTIR measurements.

Since the stabilization of the charge transfer state is crucial to this reaction, the cation identity is thought to

[1] To whom correspondence should be addressed.

0021-9517/01 $35.00

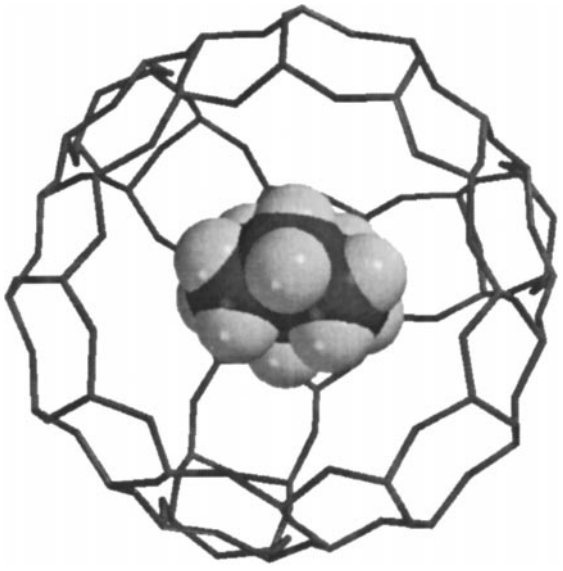

FIG.1. A zeolite Y supercage with one molecule of adsorbed cyclohexane.

play a defining role in the zeolite reactivity. Vanoppen and coworkers studied thermal cyclohexane oxidation reactions in cation-exchanged Y zeolites, CaY, SrY, BaY, and NaY (16, 17). They observed the following trend in reactivity for cyclohexane oxidation to cyclohexanone in gas and liquid phase reactions: CaY > SrY > BaY > NaY. The initial study by Vanoppen *et al*. (16), in which gas phase cyclohexane was absorbed into cation-exchanged zeolites in the presence of oxygen, concluded that, based on the cation dependence, the results were consistent with the mechanism proposed by Frei involving the formation of an alkane–oxygen charge transfer complex. However, in a later study that focused on cyclohexane oxidation using liquid cyclohexane, it was found by analysis of the reaction kinetics that a classical autoxidation process was most compatible with the data (17). It was suggested by the authors that the reactivity in the presence of a liquid phase was distinct from that of the gas phase system. Further, it was suggested that this difference could be attributed to the lower mobility of the reactant molecules within the zeolite pores at the high loadings characteristic of the liquid phase system (17). The results of these studies raise questions about the mechanism of the cyclohexane oxidation reaction at low loadings in the zeolite, typical of gas phase reaction conditions, and about how the reaction mechanism changes as a function of loading.

The objective of the current study was to examine the kinetics of the thermal and photochemical oxidation of cyclohexane in BaY and NaY using *ex situ* GC product analysis and *in situ* spectroscopic methods, such as Fourier transform infrared (FTIR) and solid state nuclear magnetic resonance (NMR), at various loadings. Although there are now several studies that support the hypothesis that the electric field at cation sites in zeolites facilitates the excitation of a $O_2 \cdot$ hydrocarbon charge transfer, the evidence also suggests that the overall forward reaction is not the sole governing factor (12, 16–21). For example, if the charge transfer state were the sole governing factor, the reaction threshold would be expected to be linearly related to the ionization potential (IP) of the hydrocarbon. However, a nonlinear relationship between the reaction threshold and the IP was observed by Frei and coworkers and has been attributed to differences in reaction quantum efficiencies (14). These changes in quantum efficiencies could be due in part to the kinetic competition between an electron transfer back reaction and the proton transfer between the cation radical and superoxide ion in the charge transfer state.

Specifically, the impact of the proton transfer rate on the oxidation process and the effect of cyclohexane loading were examined in this study. Kinetic isotope studies with deuterated cyclohexane were undertaken to determine whether the proton transfer step enters into the overall forward rate. For solution phase photoinitiated electron-transfer reactions involving the formation of alkylbenzene cation radicals, it has recently been shown that a deuterium isotope effect results when the rate of deprotonation is competitive with the rate of back electron transfer (22–24). Kinetic isotope effects between 1.5 and 5.6 have been observed, depending on the alkylbenzene and donor molecule used (22–24).

Using mixtures of normal and perdeuterated reactant molecules, kinetic studies of the thermal (35, 45, 55, 65, and 75°C) and photochemical oxidation of cyclohexane in BaY were conducted with *ex situ* product analysis using GC and GC/MS. In every case examined, the measured ratio of normal to deuterated reaction products, in the initial rate regime, showed a pronounced isotope effect. The effect of cyclohexane loading was also examined to establish a link between earlier FTIR studies of Frei and coworkers (10) and the liquid phase oxidation study of Vanoppen and coworkers (17). The activation energies for the thermal oxidation of cyclohexane in BaY and NaY were measured. *In situ* NMR and FTIR spectroscopies were used to monitor cyclohexane oxidation in the zeolite pores.

EXPERIMENTAL

Zeolite Sample Preparation

BaY was prepared from NaY (Aldrich) by standard ion-exchange procedures at 90°C using an aqueous 0.5 M $BaCl_2$ solution. The elemental composition of Al, Si, and Ba was determined by inductively coupled plasma/atomic emission spectroscopy (ICP/AES) using a Perkin–Elmer Plasma 400. The Si/Al and Ba^{2+}/Al ratios for BaY were 2.4 and 0.33, respectively.

Ex Situ Product Analysis with GC and GC/MS

Zeolites were activated in vials by heating on a vacuum rack to 300°C overnight to remove adsorbed water. The activated samples contained in vials were then placed in a glove bag filled with oxygen. The sample vials were capped and removed from the glove bag, and the desired amount of cyclohexane was injected into the vial through the septum in the cap. Control experiments, which used no zeolite in the sample vial, were also conducted. The samples were either heated in a water bath or forced air convection oven for thermal reactions or irradiated with a 500-W mercury lamp (Oriel Corp.) for photochemical reactions. A broadband long-pass filter was placed in front of the lamp for visible light excitation (Oriel Corp. filter 59472, $\%T = 0$ at 400 nm). After the reactions were completed, acetonitrile was added to the sample through the septum. The sample was stirred for 90 min. and centrifuged for 2 min. at 10,000*g*. The supernatant was then analyzed by GC or GC/MS with an FID detector and a 5% phenyl/95% methylpolysiloxane capillary column. When available, standards of the products were injected separately to determine retention times and response factors.

The calibration for quantitative analysis of the data was done in two ways. First, standard solutions of cyclohexane, cyclohexanone, and cyclohexanol in acetonitrile were prepared and a calibration curve was constructed. In addition, a second calibration curve was constructed by adding specific amounts of cyclohexane, cyclohexanone, or cyclohexanol to activated BaY. Then the hydrocarbons were extracted from BaY with acetonitrile in order to calibrate the amount of each compound that was extracted from the zeolite. The calibration with zeolite indicated that ~90% of the adsorbed cyclohexane, cylohexanone, and cylcohexanol was extracted from BaY. Cyclohexyl hydroperoxide was assumed to have the same calibration curve as the oxygenated products, cyclohexanol, and cyclohexanone. Using these two calibration curves, the mass balance was determined to range from approximately 70 to 85% in the experiments reported here. One explanation for the mass balance is that cyclohexane is lost either through leakage from the septum of the sample vial or by volatilization during the extraction process. Initial rates were calculated using kinetic data obtained at cyclohexane conversions of less than 15%.

In Situ Product Analysis with FTIR and Solid State NMR Spectroscopies

In situ FTIR spectra were recorded with a Mattson infrared spectrometer equipped with a narrowband MCT detector. Each spectrum was taken by averaging 500 scans at an instrument resolution of 4 cm^{-1}. The infrared sample cell used in this study has been described previously (25). Briefly, ~50–100 mg zeolite was coated onto a photo-etched tungsten (3×2 cm^2) grid held from a water slurry. The tungsten grid coated with the zeolite was mounted onto nickel jaws that are attached to a copper feed-through. The sample can be heated to 900°C. The temperature of the sample was measured with a thermocouple wire spotwelded to the center of the grid. The entire assembly was mounted inside of the IR cell, a $2\frac{3}{4}''$ stainless steel cube with BaF_2 windows. The IR cell was then evacuated by a turbomolecular pump to a pressure of 1×10^{-7} Torr. Zeolites were heated under vacuum at 300°C overnight to remove adsorbed water.

Cyclohexane was loaded into the zeolite by adsorption under an equilibrium vapor pressure of the liquid at room temperature. The excess hydrocarbon was pumped out for 5 min and oxygen was then added at a pressure of approximately 600 Torr. A 500-W mercury lamp (Oriel Corp.) with a water filter was used as the light source for photolysis. A broadband long-pass filter was placed in front of the lamp for visible excitation (Oriel Corp. filter 59472, $\%T = 0$ at 400 nm).

The ^{13}C NMR spectra were obtained using a wide-bore Bruker MSL-300 NMR spectrometer operating at 75.470 MHz. Cyclohexane was loaded onto BaY (~80 mg) and the sample was transferred to a 7.5-mm zirconia rotor in a glove bag containing oxygen. The sample was then heated to 85°C for 1 h. A Chemagnetics double-channel 7.5-mm pencil magic angle spinning (MAS) probe was used to spin the sample at ~5 kHz at the magic angle. Cross polarization (CP) with high-power proton decoupling was used for ^{13}C NMR signal acquisition with the following parameters: CP, contact time 2.0 ms, recycle delay 2.0 s, 90° pulse length 5.1 μs. All of the chemical shifts for ^{13}C are reported relative to TMS.

Reagents and Gases

Cyclohexane (Aldrich, 99% purity), cyclohexane-d_{12} (Cambridge Isotopes, 99%), cyclohexanone (Aldrich), and cyclohexanol (Aldrich) were used in these experiments. Acetonitrile (HPLC grade) was obtained from Fisher. All of these compounds were used without further purification. O_2 (Air Products, 99.6% purity) was also used without further purification.

RESULTS

Effect of Cyclohexane Loading on the Thermal Oxidation Reaction in BaY

The cyclohexane loading in BaY was varied in order to determine whether the cyclohexane loading level affects the thermal conversion of cyclohexane and oxygen to the three observed products, cyclohexanone, cyclohexanol, and cyclohexyl hydroperoxide. BaY samples with cyclohexane stoichiometries varied from 0.2 to 5 cyclohexane molecules/supercage were heated to 65°C for 1 h in an oxygen atmosphere and then the products were extracted from the zeolite and analyzed by GC. A graph of percent

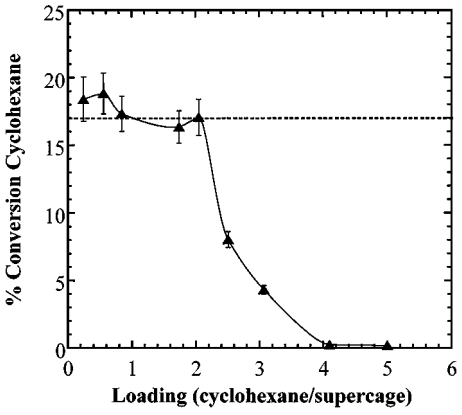

FIG. 2. Graph of the percent conversion of cyclohexane vs cyclohexane loading per supercage for the thermal oxidation of cyclohexane with molecular oxygen in BaY. The reaction conditions were 65°C for 1 h.

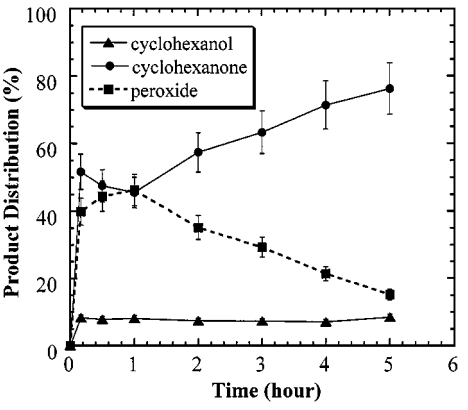

FIG. 3. Product distribution (%) vs time for the oxidation of cyclohexane (50% cyclohexane-D_{12}, 50% cyclohexane-H_{12}) and oxygen in BaY. The reaction temperature was 65°C and the loading was 1 cyclohexane/supercage.

conversion vs cyclohexane loading per supercage is presented in Fig. 2. The percent conversion is defined as the total moles of product (cyclohexanone + cyclohexanol + cyclohexyl hydroperoxide) divided by the total moles of cyclohexane added times 100. The percent conversion of cyclohexane is approximately constant at ~17% up to a loading of 2 molecules of cyclohexane/supercage. At higher loadings, the percent conversion decreases to almost 0 at a level of 4 to 5 molecules of cyclohexane added per supercage.

Kinetics of the Thermal Oxidation of Cyclohexane and Oxygen in BaY

The kinetics of the thermal oxidation of cyclohexane and oxygen in BaY were monitored as a function of temperature. For each experiment, a 1:1 molar mixture of cyclohexane-h_{12} and cyclohexane-d_{12} was injected into identical vials containing activated BaY and oxygen. The samples were equilibrated to the desired temperature and were then allowed to react for specific time periods before being quenched. The products and unreacted cyclohexane were extracted in acetonitrile and analyzed by GC. Representative kinetic plots for the thermal oxidation of a mixture of cyclohexane-H_{12}, cyclohexane-D_{12}, and oxygen in BaY at 65°C are shown in Figs. 3 and 4. The cyclohexane loading is 1 cyclohexane molecule per supercage. The product distributions for cyclohexanone, cyclohexanol, and cyclohexyl hydroperoxide formed versus time are shown in Fig. 3. The product distribution is defined as the amount of each product divided by the total products and multiplied by 100. In the first 10 min of the reaction, the amounts of cyclohexanol, cyclohexanone, and cyclohexyl hydroperoxide increase. The percentage of cyclohexanol remains approximately constant at 9% for times 10 min and greater. At times greater than 1 h, the percentage of cyclohexanone increases as the percentage of cyclohexyl hydroperoxide decreases as would be expected if cyclohexyl hydroperoxide was an intermediate that decomposed to form cyclohexanone as shown in reaction [1].

The percent conversion of cyclohexane-H_{12} and cyclohexane-D_{12} with time at 65°C at a loading of 1 cyclohexane molecule per supercage is shown in Fig. 4. Two aspects of the competitive kinetics displayed in this figure are noteworthy. First, in any given time interval more hydrogen-containing products than deuterium-containing products are obtained. Second, the decrease in the reaction rate with time shows a common rate of decrease for both isotopic labels.

The first observation is a clear indication of a substantial deuterium kinetic isotope effect in this system. Using the ratio of hydrogen- to deuterium-labeled products, at total conversions of less than 15%, the kinetic isotope

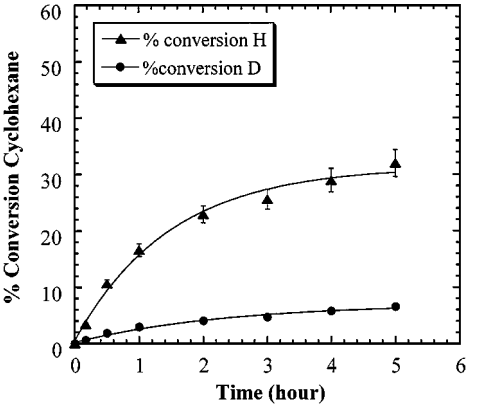

FIG. 4. Graph of the total percent conversion of cyclohexane (50% cyclohexane-D_{12}, 50% cyclohexane-H_6) to cyclohexanone, cyclohexanol, and cyclohexylhydroperoxide vs time. The cyclohexane loading was 1 cyclohexane/supercage and the reaction temperature was 65°C.

TABLE 1

Reaction conditions	Kinetic isotope effect
Thermal, 35°C	5.3
Thermal, 45°C	5.5
Thermal, 55°C	5.5
Thermal, 65°C	5.7
Thermal, 75°C	5.4
Photo, 400 nm	5.7

effect was calculated. The magnitude of the deuterium kinetic isotope effect for the oxidation of cyclohexane with oxygen in BaY at 65°C is 5.5. The deuterium isotope effects were measured at 35, 45, 55, 65, and 75°C and are listed in Table 1. The results span the range from 5.3 to 5.7 with an average of 5.5 (±0.2). The presence of a substantial deuterium kinetic isotope effect indicates that a C–H (C–D) bond is broken in the rate-determining step of reaction [1]. The partitioning between the primary versus secondary deuterium isotope effects will be discussed further under Discussion. The observation of the overall slowdown of the kinetics as the reaction proceeds is most likely due to the inhibition of the catalyst by the products. Since this inhibition depends only on the chemical identity of the products and not on their isotopic substitution, the result is an overall slowing of the reaction kinetics common to both isotopic species under these competitive reaction conditions.

The reaction is further characterized by using the temperature-dependent rate data to construct an Arrhenius plot, which is shown in Fig. 5. The initial rate at constant initial loading was determined using the linear range of the kinetic plots, which corresponded to conversions of less than 15%. Linear regression of the data yields the

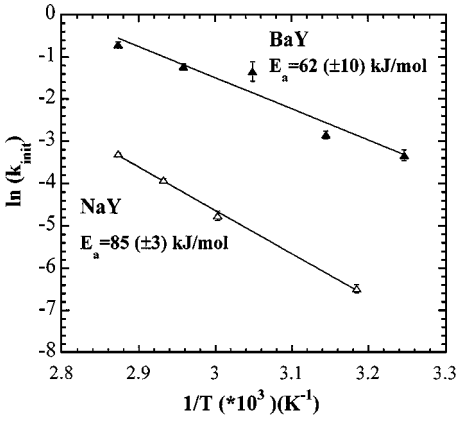

FIG. 5. Arrhenius plot of $1/T$ vs ln(initial rate) for the thermal oxidation of cyclohexane and oxygen in BaY. The cyclohexane loading was 1 cyclohexane/supercage and the reaction temperature was varied from 35 to 75°C.

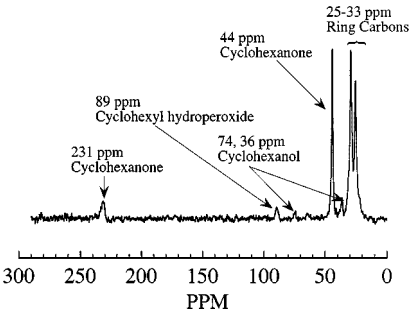

FIG. 6. ^{13}C CP/MAS with proton decoupling NMR spectrum of BaY with cyclohexane and oxygen after heating to 85°C for 1 h. The cyclohexane loading was approximately 1 cyclohexane/supercage.

activation energy, E_a, which is calculated from the slope of the best-fit line. For these experiments, the loading was constant at 1 molecule of cyclohexane per supercage. The activation energy for the reaction of cyclohexane and oxygen and BaY is determined to be 62 (±9) kJ/mol. The activation energy for the thermal oxidation of cyclohexane in NaY was also measured and was determined to be 85 (±3) kJ/mol.

In situ solid state NMR was used to directly monitor product formation in the pores of BaY after the thermal oxidation of cyclohexane. Figure 6 shows the ^{13}C solid state MAS NMR spectrum of cyclohexane (natural abundance ^{13}C) and oxygen on BaY after reacting for 1 h at 85°C. The cyclohexane loading was 1 cyclohexane molecule per supercage. ^{13}C is the only isotope of carbon that possesses a nuclear spin and its natural abundance is 1.1. After signal averaging for approximately 10 h, the ^{13}C NMR spectrum (using cross polarization and proton decoupling) shown in Fig. 6 was obtained. As expected from the GC analysis, several products were present in the zeolite pores. The C-1 carbons of cyclohexanone, cyclohexanol, and cyclohexyl hydroperoxide are easily identified by peaks at 231 ppm (C=O), 74 ppm (C–OH), and 89 ppm (COOH), respectively (26). Although not rigorously proportional to concentration due to the cross polarization used for data acquisition, a comparison of the C-2 carbon peaks of cyclohexanone (44 pm) and cyclohexanol (36 ppm) are consistent with the results of our *ex situ* GC analysis. These NMR results suggest that the higher ratio of cyclohexanol to cyclohexanone (0.5) found in our *ex situ* experiments relative to the ratio of Frei *et al*. (10) in FTIR experiments (0.02) is not an artifact of the extraction procedure used in the *ex situ* analysis. It is possible that the cyclohexanol-to-cyclohexanone branching ratio changed during the NMR experiment due to thermal reactions of the hydroperoxide during the long signal averaging required for the experiment. Substantial overlap in the ring carbon region of the spectrum (~25–33 ppm) makes interpretation of this region of the spectrum difficult. A possible peak at 64 ppm is noted and is within the range expected for a carbon singly bonded to an

oxygen; however, the low signal-to-noise ratio of this feature makes any assignment uncertain. Further, experiments using ^{13}C-labeled cyclohexane should enable more reliable conclusions regarding this feature.

Kinetics of the Photooxidation of Cyclohexane and Oxygen in BaY

The photooxidation of cyclohexane in BaY was investigated with batch reactor experiments analogous to those conducted for the thermal reaction. The cyclohexane loading in BaY was varied in order to determine whether the cyclohexane loading level affects the photooxidation of cyclohexane and oxygen to cyclohexanone, cyclohexanol, and cyclohexyl hydroperoxide. The BaY samples with cyclohexane loadings varied from 1 to 4 cyclohexane molecules per supercage were irradiated for 2 h with $\lambda > 400$ nm, and then the products were extracted from the zeolite and analyzed by GC. The conversion to cyclohexane was approximately constant at ~13% at cyclohexane loadings of 1–2 cyclohexane molecules per supercage. At loadings of 3 cyclohexane/supercage and greater, the conversion of cyclohexane decreased to almost 0. Thus, the loading effect for the photooxidation reaction is very similar to the loading effect observed in the thermal reaction.

The deuterium kinetic isotope effect for the photooxidation reaction was measured using a 1:1 molar mixture of cyclohexane-H_{12} and cyclohexane-D_{12} at a loading of 1 cyclohexane molecule per supercage. The rate for cyclohexane-D_{12} photooxidation in BaY is significantly less than the rate for cyclohexane photoxidation in BaY, indicating a substantial deuterium kinetic isotope effect, just as in the thermal reaction. The magnitude of the deuterium kinetic isotope effect for the photooxidation of cyclohexane and oxygen in BaY with $\lambda > 400$ nm is 5.7 as listed in Table 1 for comparison with the thermal results. By GC/MS, there was no evidence of H–D scrambling at the ring positions.

Photoproduct formation in the pores of BaY was monitored using *in situ* FTIR. As much as 100 mTorr of cyclohexane and 600 Torr of oxygen were loaded into BaY, and then the sample was irradiated with $\lambda > 455$ nm. A difference spectrum following the room temperature photooxidation of cyclohexane and oxygen in BaY for 22 h is shown in Fig. 7. Product peaks are observed at 1671, 1642, 1366, 1344, and 1304 cm^{-1}. The peak at 1671 cm^{-1} is assigned to the C=O mode of cyclohexanone, and the peaks at 1366 and 1344 cm^{-1} are assigned to the vibrational modes of cyclohexyl hydroperoxide (10). Both cyclohexyl hydroperoxide and cyclohexanone contribute to the peak at 1304 cm^{-1}. The shoulder at 1642 cm^{-1} is assigned to the bending modes of adsorbed water (another product of the reaction) on the zeolite. No peaks were observed that could be attributed to cyclohexanol, consistent with the results of Frei and coworkers (10).

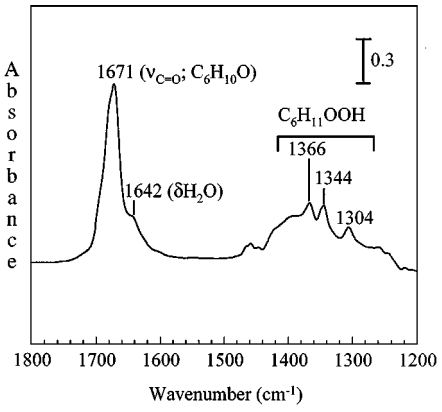

FIG. 7. Difference FTIR spectrum following the photooxidation ($\lambda >$ 455 nm) of cyclohexane and oxygen in BaY. The loading of cyclohexane was approximately 0.5 molecules of cyclohexane per supercage.

DISCUSSION

Effect of Cyclohexane Loading on the Oxidation of Cyclohexane in BaY

The cyclohexane loading influences both the thermal and photochemical oxidation of cyclohexane in BaY. For both reaction conditions, the conversion of cyclohexane decreases toward 0 at loadings greater than approximately 3 cyclohexane molecules per supercage. The absorption and dynamics of cyclohexane in the zeolite will logically contribute to such a decrease in reactivity. First, since cyclohexane is absorbed more strongly by the zeolite than oxygen, oxygen can be expected to be displaced by cyclohexane. The differential heats of adsorption for cyclohexane and oxygen in faujasite zeolites are approximately 60–77 and 16 kJ/mol, respectively (27). At maximal loadings of cyclohexane, insufficient oxygen may be present to effectively produce the critical charge transfer complex. Volumetric measurements indicate that the maximum cyclohexane loading in BaY was ~3.5 molecules/supercage, suggesting that the cutoff in the kinetics roughly corresponds to conditions of maximal cyclohexane loading. Further, molecular crowding at high loading has also been observed to decrease the molecular diffusion within zeolites. Since it is hypothesized that a diffusional step must precede charge transfer (10) as will be discussed in more detail later, a slowing of cyclohexane diffusion would similarly be expected to cause an overall slowing of reaction kinetics. In either case, it is clear that the reaction "turns off" at greater than 3 molecules of cyclohexane per supercage. Vanoppen and coworkers attributed the inhibition of the oxidation of cyclohexane in BaY in liquid phase autooxidation reactions to a similar effect (17). They suggested that the high loadings of cyclohexane in the zeolite caused a decrease in the mobility of the cyclohexane and oxidation intermediates in the pores, leading to a decrease in the oxidation reaction and causing an autoxidation

reaction mechanism to dominate under liquid phase conditions.

The decomposition of cyclohexyl hydroperoxide has been shown to lead to the formation of cyclohexanone (10). However, it is not clear how cyclohexanol is formed. One possibility is that cyclohexyl hydroperoxide reacts with cyclohexane to form 2 molecules of cyclohexanol as follows:

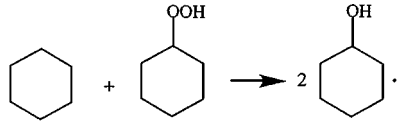

[2]

Another possibility is that the cyclohexanol is formed from the direct coupling of cyclohexyl peroxy radicals as has been suggested by Frei and coworkers (28).

Mechanism for the Photo- and Thermal Partial Oxidation of Cyclohexane in BaY

In order to probe the reaction mechanism for the photo and thermal partial oxidation of cyclohexane and oxygen in BaY, the kinetic isotope effect of the reaction was measured using mixtures of cyclohexane-H_{12} and cyclohexane-D_{12}. The results of these experiments indicate that a substantial deuterium kinetic isotope effect is operative for both the thermal and photooxidation reactions. The average overall isotope effects of 5.5($\pm$0.2) for the thermal reaction and 5.7 for the photooxidation reaction are the same within experimental error and are compatible with the view that a single-reaction mechanism operates under both thermal and photochemical reaction conditions. In a previous study of the kinetic acidity of liquid cyclohexane, the calculated total isotope effect for C_6H_{12} relative to C_6D_{12} was determined to be 6.5 ± 0.6 (29). This isotope effect includes the primary and secondary isotope effects. The total secondary isotope effect was reported to be 1.4, resulting in a primary isotope effect of $6.5/1.4 = 4.6$ (30). Using this value of 1.4 for the secondary isotope effect, the primary isotope effect for the cyclohexane oxidation reaction in BaY can be calculated to be $5.5/1.4 = 3.9$ for the thermal reaction and $5.7/1.4 = 4.1$ for the photooxidation reaction. Since both the thermal and photooxidation reactions show virtually the same isotope effect, it is likely that they share a common rate-determining step, which we suggest below to be the deprotonation of the radical cation by the superoxide anion.

The presence of a substantial deuterium isotope effect could alternatively be taken to indicate that the reaction mechanism involves direct hydrogen atom transfer in a homolytic autoxidation-type process, rather than the [hydrocarbon$^+$, O_2^-] charge transfer step indicated in reaction [1]. The activation energy for such a process can be estimated from the activation energy of the reaction of cyclohexane with tert-butylperoxy radical and is 81.5 kJ/mol (31), with a kinetic isotope effect ranging from 4.2 to 11.5, depending on the experimental conditions (32). Further, it could even be argued that the cation electric field could stabilize the dipolar structure of the transition state, which has been shown to be relevant in the oxidation of ring-substituted toluenes (32, 33) and is thought to be important in gas phase alkane-hydroxyl radical reactions (34, 35). In this way, the stabilizing effect of the electric field of the cation may be a common factor in explaining both the liquid phase and gas phase trends in catalytic reactivity, namely, CaY > SrY > BaY > NaY, that have been observed by Vanoppen and coworkers (16, 17).

However, at low cyclohexane loading, the data are more consistent with a mechanism for cyclohexane oxidation that includes charge transfer followed by a proton transfer, rather than a direct hydrogen atom transfer. Critical to this assessment is the link between the thermal and photochemical reactivity. The charge transfer intermediate was initially postulated in this system based on the observation of an absorption in the diffuse reflectance visible absorption spectrum of cyclohexane and oxygen in NaY that was consistent with an assignment to a charge transfer state (10). The correlations between the optical absorption and the photochemical reactivity, as well as the trends observed while systematically varying the exchangeable cation of the zeolite and the identity of the hydrocarbon, all support the intermediacy of a charge transfer state in the photooxidation process (10, 12). Furthermore, since the same loading effect and kinetic isotope effect were observed for both the photooxidation and thermal oxidation, it is concluded that both processes share a common mechanistic character, namely, a charge transfer intermediate state. In addition, for a homolytic abstraction mechanism, the rates would be expected to be inversely related to the C–H bond strength. This is not observed since propylene and toluene,which have weaker C–H bonds than cyclohexane, do not react thermally in cation-exchanged zeolites. Therefore, the observation of a primary kinetic isotope effect in this study suggests that the mechanism can be described by

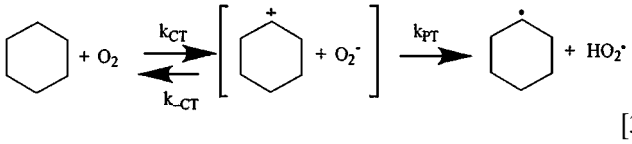

[3]

and further requires that the rate of the proton abstraction step (k_{PT}) must be slower than the rate of the back electron transfer (k_{-CT}) step. Similar reasoning was used to explain the deuterium isotope effect observed for the photoxidation of propylene to acrolein in BaY (36).

This type of reactivity parallels recent solution phase kinetic measurements of radical cation reactivity by Bockman, and coworkers (23). They demonstrated that the observation of a deuterium kinetic isotope effect of this size is also consistent with a two-step mechanism in which an

electron transfer is followed by a proton transfer, when the proton transfer must compete with the back transfer of the electron (23). They investigated fast proton transfer from various methylbenzenes to photoactivated quinones and observed a deuterium primary isotope effect of 2.4 to 5.6. While the magnitude of the isotope effect suggested that hydrogen atom transfer was the mechanism, they conclusively showed, by adding salt to trap the ionic intermediate, that the mechanism involved an electron transfer from the methylbenzene to the quinone, followed by a proton transfer step (23).

The activation energy for the thermal oxidation of cyclohexane in BaY can also be compared to solution phase measurements for proton transfer reactions from cation radicals to bases. The intrinsic barriers for proton transfer from α-substituted *p*-methoxytoluene cation radicals induced by NO_3^- and 2,6-lutidine were measured to be 51 and 63 kJ/mol, respectively, and appear to be typical of this class of reaction (37). These activation energies provide an upper bound to the activation energy expected in the cyclohexane oxidation reaction since the activation energy would be expected to be reduced in an asymmetric proton transfer reaction. In solution, radical cations of alkanes are known to be strong acids and superoxide is known to be a reasonable base. However, some caution is warranted since the electric field will strongly stabilize the charge transfer state, changing the difference in pK_a of the radical cation (38, 39) and the conjugate acid of superoxide, HO_2 (40).

A Potential Energy Profile for Cyclohexane Oxidation in Y Zeolites

Within the context of the mechanism discussed in the previous section, the potential energy profile for cyclohexane oxidation in Y zeolites can be estimated. The relative potential energies for each step of the cyclohexane oxidation reaction in BaY (NaY) are shown schematically in Fig. 8: the equilibrium configuration, the reaction precursor, the charge transfer complex, the proton transfer step, and the radical recombination step. The activation energies for the charge transfer (CT) step (forward and reverse) and for the proton transfer (PT) step are indicated by the arrows in Fig. 8.

Cation substitution, as indicated by the dashed line in Fig. 8, is assumed to primarily effect the stabilization of the charge transfer state and subsequent deprotonation. Neglecting the energies of diffusional processes and assuming a fast preequilibrium, the apparent activation energy for the cyclohexane oxidation reaction is given by $E_{\text{a,apparent}} = E_{\text{a, CT}} + E_{\text{a, PT}} - E_{\text{a,–CT}}$. The stabilization of the charge transfer complex for BaY versus NaY is indicated by the lowering of the energy of the charge transfer complex for [cyclohexane$^+$, O_2^-] in BaY relative to NaY. This is a result of the electric field present at Ba^{2+} (6.1 V/nm) cations larger than that of Na^+ (5.0 V/nm) cations in Y zeolites (19, 21, 41). The 1.1-V/nm difference in the electric field at the cation can be used to estimate the stabilization of the charge transfer complex. Using the estimates proposed by Frei and coworkers (10, 15), with cyclohexane$^+$ and O_2^- separated by 4 Å and an electric field of 1.1 V/nm (the difference between the electric field for Ba^{2+} and that for Na^+), a dipole stabilization of 0.4 eV (42 kJ/mol) can be calculated for BaY relative to NaY. Using the expression for the apparent activation energy, the dipole stabilization of the charge transfer state should result in an activation energy for BaY that is approximately 40 kJ/mol lower than that for NaY. Given the uncertainty in the estimate of the dipole stabilization energy, this model is consistent with the ~23-kJ/mol stabilization observed in the experiments reported here.

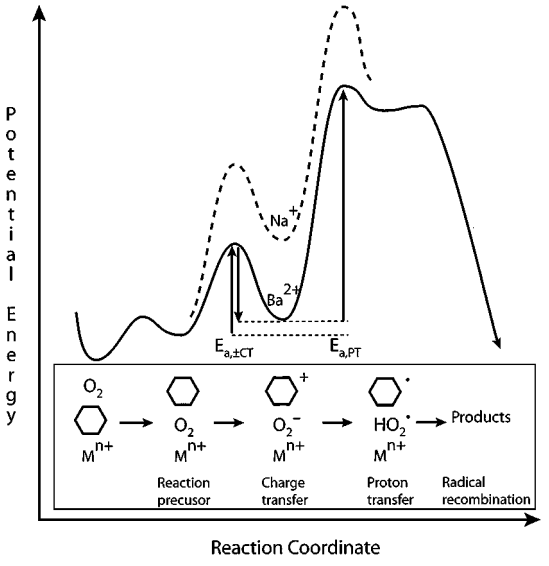

FIG. 8. A potential energy diagram for the thermal oxidation of cyclohexane in BaY (NaY) showing the relative potential energies for the equilibrium configuration, the reaction precursor, the charge transfer complex, the proton transfer step, and the radical recombination step. The relevant activation energies are also indicated by arrows. The apparent activation energy is given by $E_{\text{a, apparent}} = E_{\text{a,CT}} + E_{\text{a,PT}} - E_{\text{a,–CT}}$.

Figure 8 also illustrates the initial step of the reaction, which is diffusion of the cyclohexane and oxygen until they are aligned such that the O_2 is closest to the cation (M^{n+}) site. If we assume that the proton transfer is rate limiting and that the two mechanistic steps that precede it are in a state of preequilibrium, we can parse the experimental activation energy in BaY, 62 (±9) kJ/mol, into its component parts. Molecular dynamics studies are now capable of elucidating the details of hydrocarbon motion in faujasite-type zeolites. In one such study, Clark and coworkers have investigated the diffusion of alkanes in siliceous faujasites and have obtained an activation energy of diffusion of about 7 kJ/mol for C_6 hydrocarbons (42). This compares with an average of 14 kJ/mol from experimental measurements in Na^+-containing faujasite (42, 43). If we take the difference

to be the energy needed to remove the cyclohexane from the cation site to a favorable position on the wall of the zeolite without a proximate cation, this difference represents an estimate of the activation energy to the diffusional percursor, 7 kJ/mol. The activation energy of molecular oxygen is expected to be lower due to its small size, and a value of 3 kJ/mol will be assumed. The process of forming the reaction precursor is therefore likely to be endogodic by about 4 kJ/mol. Taking 51 kJ/mol as an estimate for the activation energy of the proton step yields a remainder of 7 kJ/mol, which we attribute to the charge transfer energy. As discussed previously by Frei and coworkers, this represents a significant stabilization of the charge transfer state by the large electric field of the cation in the zeolite (11–13, 15, 44). In the gas phase, the energy of the radical pair (cyclohexyl radical and HO_2 radical) lies 197 kJ/mol higher than that of the cyclohexane and oxygen reactants (45). The zeolite will certainly cause some stabilization of the radical pair due to adsorption and polarization effects, leading to an energy state slightly below the proton transfer barrier. Although our discussion only provides a rough estimate of the relevant energies, this model as represented in Fig. 8 appears to be compatible with the experimental observations to date.

This energy profile also predicts that the overall forward rate can be significantly affected by the activation energy for hydrocarbon diffusion. Thus, the experimental observation that toluene exhibits no thermal reactivity under conditions analogous to those used for the study of cyclohexane oxidation is consistent with the large energy required to displace toluene from a cation site (40 and 66 kJ/mol for NaY (46) and Ca-LSX (47), respectively) compared to cyclohexane ($\sim$7 kJ/mol). Photooxidation in zeolites, however, is observed for the toluene system even at low temperatures (19, 48, 49). This is interpreted as indicating that the lower energy reaction precursor configurations are able to be activated by a visible photon; that is to say, the hydrocarbon is more closely associated with the cation, leading to less stabilization of the charge transfer state. The impact of the large activation energy required, associated with strongly adsorbed molecules, may also be responsible for the selectivity in these systems, since oxygenates are expected to be strongly absorbed at the zeolite cation sites. Thus, even for oxygenates that would be expected to oxidize more easily than the parent molecule, oxidation may be precluded by the inability of the strongly absorbed molecule to form the diffusional precursor state.

CONCLUSIONS

The kinetics of the photo and thermal oxidation of cyclohexane and oxygen in BaY were investigated using *ex situ* GC and *in situ* NMR and FTIR spectroscopies. The conversion of cyclohexane to cyclohexanone, cyclohexanol, and cyclohexyl hydroperoxide decreased dramatically for loadings greater than 3 cyclohexane molecules per supercage. This was attributed to decreased diffusion of cyclohexane and oxygen in the zeolite pores. A substantial deuterium kinetic isotope effect was observed for both the photo- and thermal oxidation of cyclohexane. The activation energies of cyclohexane oxidation in BaY and NaY were measured to be 62 ($\pm$9) and 85 ($\pm$3) kJ/mol, respectively. Several mechanistic implications were deduced from the measured isotope effects and energetics.

ACKNOWLEDGMENTS

Although the research described in this article has been funded wholly or in part by the Environmental Protection Agency through Grant R825304-01-0 to S.C.L. and V.H.G., it has not been subjected to the Agency's required peer and policy review and therefore does not necessarily reflect the views of the Agency and no official endorsement should be inferred. A. R. Leone, M. El-Maazawi, and Gonghu Li are acknowledged for assistance with experiments.

REFERENCES

1. Suresh, K. A., Sharma, M. M., and Sridhar, T., *Ind. Eng. Chem. Res.* **39**, 3958 (2000).
2. Parshall, G. W., and Ittel, S. D., "Homogeneous Catalysis," 2nd ed. Wiley, New York, 1992.
3. Sheldon, R., " The Chemistry of Peroxides." Wiley, New York, 1983.
4. Arends, I. W. C. E., Sheldon, R. A., Wallau, M., and Schuchardt, U., *Angew. Chem. Int. Ed. Engl.* **36**, 1144 (1997).
5. Raja, R., Sankar, G., and Thomas, J. M., *J. Am. Chem. Soc.* **121**, 11,926 (1999).
6. Chen, J. D., and Sheldon, R. A., *J. Catal.* **153**, 1 (1995).
7. Vanoppen, D. L., Devos, D. E., Genet, M. J., Rouxhet, P. G., and Jacobs, P. A., *Angew. Chem. Int. Ed. Engl.* 560 (1995).
8. Lu, G. X., Gao, H. X., Suo, J. H., and Li, S. B., *J. Chem. Soc., Chem. Commun.* **21**, 2423 (1994).
9. Pires, E. L., Magalhaes, J. C., and Schuchardt, U., *Appl. Catal. A: General* **203**, 231 (2000).
10. Sun, H., Blatter, F., and Frei, H., *J. Am. Chem. Soc.* **118**, 6873 (1996).
11. Frei, H., Blatter, F., and Sun, H., *Chemtech.* 24 (1996).
12. Blatter, F., Sun, H., and Vasenkov, S., Frei, H., *Catal. Today* **41**, 297 (1998).
13. Blatter, F., and Frei, H., *J. Am. Chem. Soc.* **115**, 7501 (1993).
14. Blatter, F., and Frei, H., *J. Am. Chem. Soc.* **116**, 1812 (1994).
15. Blatter, F., Moreau, F., and Frei, H., *J. Phys. Chem.* **98**, 13,403 (1994).
16. Vanoppen, D. L., DeVos, D. E., and Jacobs, P. A., *Stud. Surf. Sci. Catal.* **105**, 1045 (1996).
17. Vanoppen, D. L., DeVos, D. E., and Jacobs, P. A., *J. Catal.* **177**, 22 (1998).
18. Li, P., Xiang, Y., Grassian, V. H., and Larsen, S. C., *J. Phys. Chem. B* **103**, 5058 (1999).
19. Panov, A. G., Larsen, R. G., Totah, N. I., Larsen, S. C., and Grassian, V. H., *J. Phys. Chem. B* **104**, 5706 (2000).
20. Xiang, Y., Larsen, S. C., and Grassian, V. H., *J. Am. Chem. Soc.* **121**, 5063 (1999).
21. Myli, K. B., Larsen, S. C., and Grassian, V. H., *Catal. Lett.* **48**, 199 (1997).
22. Fujita, M., Ishida, A., Takamuku, S., and Fukuzumi, S., *J. Am. Chem. Soc.* **118**, 8566 (1996).
23. Bockman, T. M., Hubig, S. M., and Kochi, J. K., *J. Am. Chem. Soc.* **120**, 2826 (1998).
24. Lewis, F. D., and Petisce, J. R., *Tetrahedron* **42**, 6207 (1986).
25. Miller, T. M., and Grassian, V. H., *J. Am. Chem. Soc.* **117**, 10,969 (1995).

26. Barton, D. H. R., Csuhai, E., Doller, D., and Balavoine, G., *J. Chem. Soc., Chem. Commun.* 1787 (1990).
27. Breck, D. W., "Zeolite Molecular Sieves." Wiley, New York, 1974.
28. Sun, H., Blatter, F., and Frei, H., *Catal. Lett.* **44**, 247 (1997).
29. Streitweiser, Jr., A., Young, W. R., and Caldwell, R. A., *J. Am. Chem. Soc.* **91**, 527 (1969).
30. Dixon, R. E., and Streitweiser, A. J., *J. Org. Chem.* **57**, 6125 (1992).
31. Chenier, J. H. B., Tong, S. B., and Howard, J. A., *Can. J. Chem.* **56**, 3047 (1978).
32. Howard, J. A., *in* "Free Radicals" (J. K. Kochi, Ed.), Vol. 2, p. 3. Wiley, New York, 1973.
33. Ingold, K. U., *Acc. Chem. Res.* **2**, 1 (1969).
34. Clarke, J. S., Kroll, J. H., Donahue, N. M., and Anderson, J. G., *J. Phys. Chem. A* **102**, 9847 (1998).
35. Donahue, N. M., Clarke, J. S., and Anderson, J. G., *J. Phys. Chem. A* **102**, 3923 (1998).
36. Blatter, F., Sun, H., and Frei, H., *Catal. Lett.* **35**, 1 (1995).
37. Baciocchi, E., Del Giacco, T., and Elisei, F., *J. Am. Chem. Soc.* **115**, 12,290 (1993).
38. Hammerich, O., and Parker, V. D., *Adv. Phys. Org. Chem.* **20**, 55 (1984).
39. Mella, M., Freccero, M., and Albini, A., *Tetrahedron* **52**, 5533 (1996).
40. Bielski, B. H. I., Cabelli, D. E., Arudi, R. L., and Ross, A. B., *J. Phys. Chem. Ref. Data* **14**, 1041 (1985).
41. Bordiga, S., Lamberti, C., Geobaldo, F., and Zecchina, A., *Langmuir* **11**, 527 (1995).
42. Clark, L. A., Ye, G. T., Gupta, A., Hall, L. L., and Snurr, R. Q., *J. Chem. Phys.* **111**, 1209 (1999).
43. Karger, J., Pfeifer, H., Rauscher, M., and Walter, A., *I.C.S. Faraday I* **76**, 717 (1980).
44. Vasenkov, S., and Frei, H., *J. Phys. Chem. B* 4539 (1997).
45. Tolman, C. A., Druliner, J. D., Nappa, M. J., and Herron, N., *in* "Activation and Functionalization of Alkanes" (C. L. Hill, Ed.), Chap. 10. Wiley, New York, 1989.
46. Isfort, O., Boddenberg, B., Fujara, F., and Grosse, R., *Chem. Phys. Lett.* **288**, 71 (1998).
47. Schaefer, D. J., Favre, D. E., Wilhelm, M., Weigel, S. J., and Chmelka, B. F., *J. Am. Chem. Soc.* **119**, 9252 (1997).
48. Panov, A. G., Myli, K. B., Xiang, Y., Grassian, V. H., and Larsen, S. C., *in* "Green Chemical Syntheses and Processes" (P. Anastas, L. G. Heine, T. C. Williamson, Eds.), p. 206. Am. Chem. Soc., Washington, DC, 2000.
49. Sun, H., Blatter, F., and Frei, H., *J. Am. Chem. Soc.* **116**, 7951 (1994).